



New fluorescence-based high-throughput screening assay for small molecule inhibitors of tyrosyl-DNA phosphodiesterase 2 (TDP2)



Carlos J.A. Ribeiro^a, Jayakanth Kankanala^a, Ke Shi^b, Kayo Kurahashi^b, Evgeny Kiselev^c, Azhar Ravji^c, Yves Pommier^c, Hideki Aihara^b, Zhengqiang Wang^{a,*}

^a Center for Drug Design, Academic Health Center, University of Minnesota, Minneapolis, MN 55455, United States

^b Department of Biochemistry, Molecular Biology and Biophysics, University of Minnesota, Minneapolis, MN 55455, United States

^c Developmental Therapeutics Branch and Laboratory of Molecular Pharmacology, Center for Cancer Research, National Cancer Institute, National Institutes of Health, Bethesda, MD 20892, United States

ARTICLE INFO

Keywords:

Tyrosyl-DNA phosphodiesterase 2 (TDP2)

Anti-cancer

Fluorescence assay

High-throughput screening (HTS)

Virtual screening

Guanidines

ABSTRACT

Tyrosyl-DNA phosphodiesterase 2 (TDP2) repairs topoisomerase II (TOP2) mediated DNA damages and causes resistance to TOP2-targeted cancer therapy. Inhibiting TDP2 could sensitize cancer cells toward TOP2 inhibitors. However, potent TDP2 inhibitors with favorable physicochemical properties are not yet reported. Therefore, there is a need to search for novel molecular scaffolds capable of inhibiting TDP2. We report herein a new simple, robust, homogenous mix-and-read fluorescence biochemical assay based using humanized zebrafish TDP2 (14M_zTDP2), which provides biochemical and molecular structure basis for TDP2 inhibitor discovery. The assay was validated by screening a preselected library of 1600 compounds ($Z' \geq 0.72$) in a 384-well format, and by running in parallel gel-based assays with fluorescent DNA substrates. This library was curated via virtual high throughput screening (vHTS) of 460,000 compounds from Chembridge Library, using the crystal structure of the novel surrogate protein 14M_zTDP2. From this primary screening, we selected the best 32 compounds (2% of the library) to further assess their TDP2 inhibition potential, leading to the IC_{50} determination of 10 compounds. Based on the dose-response curve profile, pan-assay interference compounds (PAINS) structure identification, physicochemical properties and efficiency parameters, two hit compounds, **11a** and **19a**, were tested using a novel secondary fluorescence gel-based assay. Preliminary structure-activity relationship (SAR) studies identified guanidine derivative **12a** as an improved hit with a 6.4-fold increase in potency over the original HTS hit **11a**. This study highlights the importance of the development of combination approaches (biochemistry, crystallography and high throughput screening) for the discovery of TDP2 inhibitors.

1. Introduction

Tyrosyl-DNA phosphodiesterase 2 (TDP2), also known as TNF receptor associated factor (TRAF) and TNF receptor associated protein (TTRAP) (Pype et al., 2000) and ETS1-associated protein 2 (EAPII) (Pei et al., 2003), was the first human 5'-tyrosyl DNA phosphodiesterase identified (Cortes Ledesma et al., 2009). TDP2 plays a major role in DNA repair by specifically cleaving the 5'-tyrosyl-DNA phosphodiester bond of stalled topoisomerase II (TOP2) cleavage complexes [reviewed in (Menon and Povirk, 2016; Pommier et al., 2014)].

TOP2 resolves topological problems with double-stranded DNA during normal physiological processes, such as transcription and replication. Mechanistically, TOP2 acts by generating TOP2-DNA cleavage complexes (TOP2cc) featuring a covalent phosphotyrosine linkage between its active site tyrosine and the 5' phosphate end at the site of

DNA cleavage. These complexes are transient as TOP2 reseals cleaved DNA at the end of its catalytic cycle (Pommier et al., 2016). However, under certain conditions, such as exposure to TOP2 poisons, TOP2cc become abortive (Fortune and Osheroff, 2000; Nitiss, 2009; Pommier, 2013). Repair of abortive TOP2cc by cellular DNA repair machinery, particularly TDP2, can lead to cancer resistance to TOP2 poisons. By inhibiting TDP2, cancer cells could be sensitized toward treatment with TOP2 poisons, resulting in therapeutic efficacy with much lower doses of TOP2 poisons (Marchand et al., 2016).

Several lines of evidence support the potential clinical benefits of specifically targeting TDP2 in cancer therapy: (i) TDP2-deleted cells show hypersensitivity to TOP2 poisons (Cortes Ledesma et al., 2009; Zeng et al., 2011); (ii) TDP2 knockout vertebrate cells show normal cell growth and knockout mice are viable without noticeable pathology, suggesting that TDP2 inhibitors could be well tolerated (Gomez-

* Corresponding author.

E-mail address: wangx472@umn.edu (Z. Wang).

Herreros et al., 2013); (iii) the oncogenic role of overexpressed TDP2 has been established in several non-small-cell lung carcinoma cells (Li et al., 2011), and TDP2 up-regulation attained by p53 gain-of-function mutation has been linked to TOP2 poison resistance in human lung cancer (Do et al., 2012); and (iv) tumor cells frequently lack parallel DNA repair pathways, which makes them more vulnerable to certain cancer chemotherapy (principle of synthetic lethality) (Curtin, 2012), and more specifically to TOP2 inhibitors (Hoa et al., 2016; Maede et al., 2014; Pommier et al., 2014).

In addition, TDP2 is also implicated in picornavirus and hepatitis B virus (HBV) infections during steps where cleavage of a 5'-phosphotyrosine covalent bond occurs. In particular, picornavirus uses TDP2, also known as VPg-unlinkase, to release the viral genomic RNA from VPg protein necessary during RNA replication (Maciejewski et al., 2016; Virgen-Slane et al., 2012). HBV uses the DNA repair machinery of the infected cells to convert viral genomic relaxed circular DNA (RC-DNA) into covalently closed circular DNA (cccDNA) where TDP2 could play a role in releasing the viral P-protein from the 5' end of RC-DNA (Koniger et al., 2014).

Since the discovery of TDP2 in 2009 (Cortes Ledesma et al., 2009), only a few scaffolds have been identified possessing TDP2 inhibitory activity (Laev et al., 2016): compound **1** (Ro 08-2750, Fig. 1) (Thomson et al., 2013), deazaflavins (e.g. **2**) (Hornyak et al., 2016; Marchand et al., 2016; Raouf et al., 2013), isoquinoline-1,3-diones (e.g. **3**) (Kankanala et al., 2016), the triple inhibitors TOP1/TDP1/TDP2 indenoisoquinolines (e.g. **4**) (Beck et al., 2016; Wang et al., 2017), compounds **5** (NSC375986), **6** (NSC114532) (Kossmann et al., 2016) and **7** (NSC111041) (Kont et al., 2016). Deazaflavin derivatives are the only described TDP2 inhibitors with activities in the nanomolar range. However, their use as molecular probes in studying cellular functions and their potential as drug candidates are severely hindered by the poor cell permeability. (Hornyak et al., 2016). Therefore, new scaffolds with good potencies and desirable physicochemical properties are highly desired.

The first reported methods developed to biochemically measure TDP2 activity employed gel-based assays (Cortes Ledesma et al., 2009; Gao et al., 2012; Zeng et al., 2011). In addition to using radiolabeled-substrates, these assays can be expensive and time-consuming, and thus may not be suitable for high-throughput screening (HTS). Colorimetric assays using T5NPP (Adhikari et al., 2011) or NPPP (Raouf et al., 2013; Thomson et al., 2013) as substrate have been developed, though difficulties in achieving enzyme inhibition above 75% were observed when NPPP was employed, and high enzyme concentration (30–36 nM) was

required for both chromogenic assays. Since TDP2 prefers more physiologically relevant 5'-phosphotyrosyl oligonucleotides substrates over the small compound surrogates (Gao et al., 2012), a new colorimetric assay using a DNA substrate was reported (Thomson et al., 2013). However, this particular assay required the addition of calf intestinal alkaline phosphatase (CIP) to cleave the phosphate group necessary for the reaction development. Recently, Hornyak et al. reported a fluorescence-based assay using a 13-mer oligonucleotide substrate with a 5'-tyrosine conjugated with FITC fluorophore and an enzyme concentration much lower than the chromogenic assays (50 pM) (Hornyak et al., 2016). However, the TR-FRET nature of this assay required the addition of trivalent metal ion sensor (Gyrasol technologies) to quench the fluorescence of the substrate while stopping the reaction, resulting in increased assay costs, and allowing only end-point quenched readings.

We report herein a new fluorescence-based assay allowing reading in both continuous and quenched modality. With quenched reaction protocol this new assay is amenable for HTS and requires low enzyme concentration. In addition, the continuous reaction reading allows easy detection of false positives due to the presence of fluorescent compounds, as well as kinetic data collection (Acker and Auld, 2014). By employing a humanized zebrafish protein (14M_zTDP2) developed by our group, and whose crystal structure is included in this report, we screened a library of 1600 compounds preselected via virtual high-throughput screening (vHTS).

2. Materials and methods

2.1. Chemistry

All commercial chemicals were used as supplied unless otherwise indicated. Flash chromatography was performed on a Teledyne Combiflash RF-200 with RediSep columns (silica) and indicated mobile phase. All moisture sensitive reactions were performed under an inert atmosphere of ultrapure argon with oven-dried glassware. ^1H and ^{13}C NMR spectra were recorded on a Varian 600 MHz or Bruker 400 spectrometer. Mass data were acquired on an Agilent 6230 TOF LC/MS spectrometer capable of ESI and APCI ion sources. All tested compounds have a purity $\geq 95\%$.

2.1.1. General procedural for synthesis of 2, 2, 4-trimethyl dihydroquinolines (10)

To a solution of corresponding aniline **8** (10 mmol) in acetone (15 mL), was added catalytic InCl_3 (5 mol%) and the resulting mixture

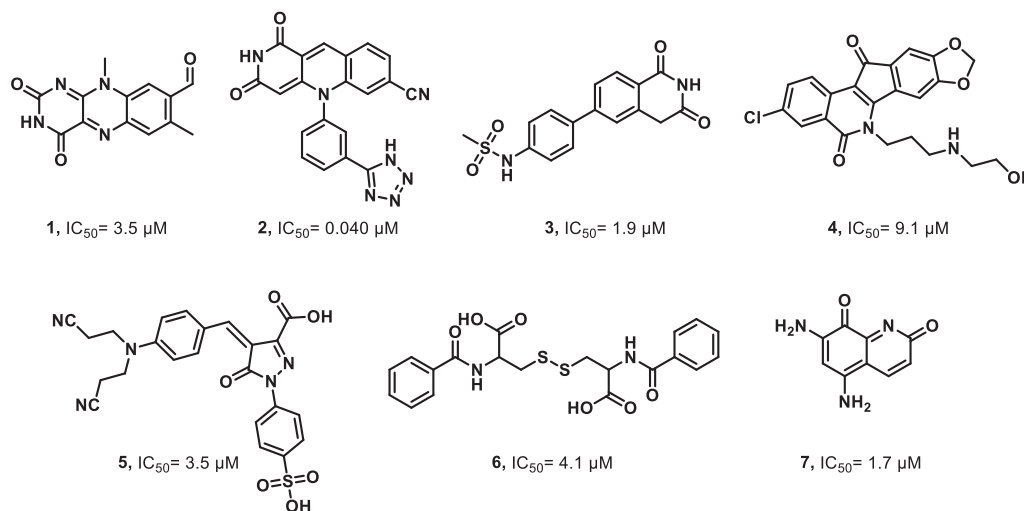


Fig. 1. Representative reported TDP2 inhibitors.

was stirred at 50 °C for 12–24 h. The solvent was removed in vacuo and the crude was dissolved in CH₂Cl₂, washed with Na₂CO₃ solution and brine, dried over Na₂SO₄ and evaporated in vacuo to produce the crude product. Purification of the crude product using Combi flash with 0–40% hexane in ethyl acetate as eluent furnished the desired product in 40–65% yield. Adapted from (Li et al., 2015).

2.1.1.1. 6-Methoxy-2,2,4-trimethyl-1,2-dihydroquinoline (10a). Yield: 40%; ¹H NMR (600 MHz, DMSO-*d*₆) δ 6.59–6.52 (m, 2H), 6.41 (d, *J* = 9.0 Hz, 1H), 5.38 (s, 1H), 5.31 (s, 1H), 3.64 (s, 3H), 1.88 (d, *J* = 0.8 Hz, 3H), 1.16 (s, 6H).

2.1.1.2. 6-Chloro-2,2,4-trimethyl-1,2-dihydroquinoline (10c) (Li et al., 2006). Yield: 65%; ¹H NMR (600 MHz, CDCl₃) δ 7.00 (s, 1H), 6.92 (d, *J* = 8.3 Hz, 1H), 6.36 (d, *J* = 7.7 Hz, 1H), 5.35 (s, 1H), 3.11 (s, 1H), 1.96 (s, 3H), 1.27 (s, 6H).

2.1.2. General procedural for synthesis of substituted quinazolines (11)

To a solution of **10** (2.46 mmol) in water (5 mL), was added cyanoguanidine (2.46 mmol), concentrated HCl (1 mL) and the resulting mixture was stirred under reflux for 4 h. The hot mixture was decanted from oils, cooled and stirred continuously by treating with concentrated KOH until a pH of 10–11 was obtained. The resulting precipitate was filtered and washed several times with isopropanol followed by recrystallization from ethanol gave the desired product in 55–62% yield. Adapted from (Rosowsky and Modest, 1972; Webb et al., 2003).

2.1.2.1. 1-(6-Methoxy-4-methylquinazolin-2-yl) guanidine (11a). Yield: 55%; ¹H NMR (600 MHz, DMSO-*d*₆) δ 7.51 (d, *J* = 9.0 Hz, 1H), 7.37 (d, *J* = 9.1 Hz, 1H), 7.28 (s, 1H), 7.07 (s, 2H), 3.87 (s, 3H), 2.71 (s, 3H). ¹³C NMR (150 MHz, DMSO-*d*₆) δ 167.4, 159.3, 155.1, 145.9, 127.7, 125.2, 119.7, 104.3, 55.8, 22.0. HRMS-ESI (+) *m/z* calculated for C₁₁H₁₄N₅O, 232.1198 [M + H]⁺; found: 232.1196.

2.1.2.2. 1-(6-Ethoxy-4-methylquinazolin-2-yl) guanidine (11b) (Brown, 1965). Yield: 62%; ¹H NMR (600 MHz, DMSO-*d*₆) δ 7.50 (d, *J* = 9.1 Hz, 1H), 7.35 (dd, *J* = 9.1, 2.6 Hz, 1H), 7.27 (d, *J* = 2.6 Hz, 1H), 6.98 (s, 2H), 4.13 (q, *J* = 6.9 Hz, 2H), 2.69 (s, 3H), 1.38 (t, *J* = 6.9 Hz, 3H). ¹³C NMR (100 MHz, DMSO-*d*₆) δ 167.0, 159.0, 154.0, 145.5, 127.3, 125.1, 119.4, 104.8, 63.6, 21.7, 14.7. HRMS-ESI (+) *m/z* calculated for C₁₂H₁₆N₅O, 246.1349 [M + H]⁺; found: 246.1340.

2.1.2.3. 1-(6-Chloro-4-methylquinazolin-2-yl) guanidine hydrochloride (11c) (Theiling and McKee, 1952). Yield: 58%; ¹H NMR (600 MHz, DMSO-*d*₆) δ 11.39 (s, 1H), 10.91 (s, 1H), 8.19 (s, 3H), 8.12 (d, *J* = 9.0 Hz, 1H), 8.07 (d, *J* = 2.3 Hz, 1H), 7.71 (dd, *J* = 9.0, 2.3 Hz, 1H), 2.67 (s, 3H). ¹³C NMR (150 MHz, DMSO-*d*₆) δ 201.8, 155.6, 151.7, 136.8, 133.9, 131.2, 127.7, 126.9, 123.5, 29.2. HRMS-ESI (+) *m/z* calculated for C₁₀H₁₁ClN₅, 236.0697 [M + H]⁺; found: 236.0696.

2.1.3. 2-((6-Methoxy-4-methylquinazolin-2-yl) amino)-5, 6-dimethylpyrimidin-4(3H)-one (12a)

To a solution of **11a** (0.10 g, 0.43 mmol) in minimal hot DMSO, was added ethyl 2-methylacetoacetate (0.07 mL, 0.52 mmol) and NaHCO₃ (0.044 g, 0.52 mmol). The reaction mixture was heated at 170 °C until the disappearance of starting material. The solution was cooled, and water was added to precipitate the product which was collected by filtration, washed with acetone and water and dried to afford **12a** (0.04 g, 30%) as a tan solid. ¹H NMR (600 MHz, DMSO-*d*₆) δ 13.28 (s, 1H), 11.00 (s, 1H), 7.70 (d, *J* = 9.0 Hz, 1H), 7.60 (dd, *J* = 9.1, 2.7 Hz, 1H), 7.48 (d, *J* = 2.5 Hz, 1H), 3.93 (s, 3H), 2.87 (s, 3H), 2.18 (s, 3H), 1.90 (s, 3H). HRMS-ESI (+) *m/z* calculated for C₁₆H₁₈N₅O₂, 312.1460 [M + H]⁺; found: 312.1461. Adapted from (LaPorte et al., 2014).

2.1.4. 2-((6-Methoxy-4-methylquinazolin-2-yl) amino) quinazolin-4(3H)-one (12b) (Guiles et al., 2009)

A mixture of **11a** (0.05 g, 0.22 mmol) and anthranilic acid (0.04 g, 0.26 mmol) in 1 mL of DMSO was heated at 170 °C until the starting material disappeared. The reaction mixture was cooled, water was added, and the resulting product was filtered and washed with excess water. The crude mixture was recrystallized from chloroform to yield the desired product as colorless crystals (0.046 g, 64%). ¹H NMR (600 MHz, DMSO-*d*₆) δ 13.60 (s, 1H), 11.11 (s, 1H), 8.04 (d, *J* = 7.7 Hz, 1H), 7.77–7.69 (m, 2H), 7.60 (dd, *J* = 9.1, 2.7 Hz, 1H), 7.47 (t, *J* = 7.6 Hz, 2H), 7.30 (t, *J* = 7.4 Hz, 1H), 3.92 (s, 3H), 2.89 (s, 3H). HRMS-ESI (+) *m/z* calculated for C₁₈H₁₆N₅O₂, 334.1304 [M + H]⁺; found: 334.1307. Adapted from (Shikhaliev et al., 2003).

2.1.5. 1-(6-Methoxy-4-oxo-3,4-dihydroquinazolin-2-yl)guanidine (15)

To a solution of anthranilic acid (0.1 g, 0.59 mmol) in 1 mL of 10% H₂SO₄, was added cyanoguanidine (0.075 g, 0.89 mmol) and refluxed for 60 min. The hot solid was precipitated and washed with excess water to furnish the desired product as colorless solid (0.077 g, 55%). ¹H NMR (600 MHz, DMSO-*d*₆) δ 11.12 (s, 1H), 7.48 (s, 2H), 7.35 (d, *J* = 2.7 Hz, 1H), 7.31 (d, *J* = 8.8 Hz, 1H), 7.22 (dd, *J* = 8.8, 2.7 Hz, 1H), 3.80 (s, 3H). HRMS-ESI (+) *m/z* calculated for C₁₀H₁₂N₅O₂, 234.0991 [M + H]⁺; found: 234.0994.

2.1.6. 4-Amino-5-(furan-2-yl)-2,4-dihydro-3H-1,2,4-triazole-3-thione (18) (Koparr et al., 2004)

To a solution of KOH (0.67 g, 11.89 mmol) in methanol (10 mL), was added furoic hydrazide (1.0 g, 7.92 mmol), CS₂ (0.72 mL, 11.89 mmol) and stirred at room temperature for 24 h and then ether was added and stirred the reaction mixture for another 2 h. The resulting solid was filtered, washed with cold methanol and ether and air dried. The solid was refluxed in excess of hydrazine hydrate (10 eq) for 5 h, cooled and poured into the acidic water (pH = 2). The solid was filtered and recrystallized from ethanol to produce the desired compound as colorless crystals (1.01 g, 70% over two steps). ¹H NMR (600 MHz, DMSO-*d*₆) δ 13.92 (s, 1H), 7.94 (dd, *J* = 1.8, 0.6 Hz, 1H), 7.39 (dd, *J* = 3.5, 0.6 Hz, 1H), 6.73 (dd, *J* = 3.5, 1.8 Hz, 1H), 5.83 (s, 2H). Adapted from (Khan et al., 2016).

2.1.7. General procedure for the synthesis of 3-(furan-2-yl)-6-phenyl-[1,2,4]triazolo[3,4-b][1,3,4]thiadiazole derivatives (19)

To a mixture of **18** (1.0 mmol) in POCl₃ (5 mL), was added substituted benzoic acid (1.1 mmol) and refluxed for 6 h. The reaction mixture was cooled and slowly poured into crushed ice with stirring and neutralized with sodium bicarbonate. The precipitated solid was filtered, washed with cold water, dried, and recrystallized from ethanol to afford the desired compounds (**19**) as colorless crystals in 53–70% yield. Adapted from (Khan et al., 2016).

2.1.7.1. 6-(3,4-Dimethylphenyl)-3-(furan-2-yl)-[1,2,4]triazolo[3,4-b][1,3,4]thiadiazole (19a). Yield: 53%; ¹H NMR (600 MHz, DMSO-*d*₆) δ 8.04 (s, 1H), 7.84 (s, 1H), 7.78 (d, *J* = 7.6 Hz, 1H), 7.41 (t, *J* = 6.4 Hz, 2H), 6.82 (s, 1H), 2.35 (s, 3H), 2.33 (s, 3H). ¹³C NMR (150 MHz, DMSO-*d*₆) δ 167.5, 145.4, 142.5, 140.1, 139.3, 138.1, 130.6, 127.8, 126.5, 124.8, 112.2, 111.8, 19.60, 19.18. HRMS-ESI (+) *m/z* calculated for C₁₅H₁₃N₄OS, 297.0810 [M + H]⁺; found: 297.0813.

2.1.7.2. 3-(Furan-2-yl)-6-(2-methoxyphenyl)-[1,2,4]triazolo[3,4-b][1,3,4]thiadiazole (19b) (Zhang et al., 2002). Yield: 70%; ¹H NMR (600 MHz, DMSO-*d*₆) δ 8.32 (dd, *J* = 7.9, 1.5 Hz, 1H), 8.02 (dd, *J* = 1.6, 0.5 Hz, 1H), 7.74–7.56 (m, 1H), 7.41 (d, *J* = 3.5 Hz, 1H), 7.35 (d, *J* = 8.4 Hz, 1H), 7.21 (t, *J* = 7.6 Hz, 1H), 6.81 (dd, *J* = 3.4, 1.8 Hz, 1H), 4.06 (s, 3H). ¹³C NMR (150 MHz, DMSO-*d*₆) δ 162.5, 157.1, 154.8, 145.2, 140.2, 138.6, 134.4, 127.9, 121.7, 116.8, 113.1, 112.2, 111.3, 56.5. HRMS-ESI (+) *m/z* calculated for C₁₄H₁₁N₄O₂S, 299.0603 [M + H]⁺; found: 299.0606.

2.2. Curation of screening compounds

Structure based virtual screening (VS) is routinely performed in drug discovery involving in hit identification as a complementary approach to HTS which requires enormous cost, time and resources etc. A computational docking tool “Glide” (Friesner et al., 2004; Schrödinger, 2014b) from Schrodinger suite 2014-3 was used to perform virtual screening of larger commercial libraries which offers speed and accuracy in binding mode predictions and providing consistently high enrichment at every level. The docking protocol involves several steps which includes a) protein preparation: The crystal structure of zH2TDP2^{cat} (14M_zTDP2^{cat}) was used for protein preparation in which bond orders and missing side chains were corrected, polar hydrogens are added, metal binding states were predicted, and the protein was minimized (pdb code: 6CA4). b) ligand preparation involving applying protonation and tautomeric states to the compounds from Chembridge library using lig prep (Schrödinger, 2014a) and Epik; c) Grid generation: creating a grid around the metal ions (Mn²⁺) in the catalytic site and imposing a pharmacophore constraint with the metal ion to improve the chances of success in finding a hit molecule and d) docking of small molecule library (460 K) to the prepared protein of interest. The compound library (460 K) was first docked and ranked in Glide vHTS mode. The top 115 K molecules (25%) from vHTS mode were then docked and ranked using standard precision (SP) Glide (Friesner et al., 2004). The resultant top 28,750 (25%) compounds from SP mode were then docked and ranked using the more accurate and computationally intensive extra-precision (XP) mode (Friesner et al., 2006). The top 7200 compounds were selected for visual inspection and by applying a stringent constraint of physicochemical properties and synthetic tractability, we created a small sub-set of 1600 compounds for purchasing and biological evaluation. The screening protocol reported above was routinely and effectively utilized in the structure based virtual screening to aid hit-identification of various drug targets (Cain et al., 2014; Ravindranathan et al., 2010; Simmons et al., 2010; Umamaheswari et al., 2010).

2.3. Biology

Compound library of 1600 compounds was purchased from Chembridge. Stock solutions between 2 and 20 mM were initially prepared and then sets of 320 compounds were plated and stored into 384-well plates at 2 mM in DMSO, mimicking the final HTS layout. Before screening, an intermediate plate was prepared consisting of compounds at 100 μ M in reaction buffer. Substrate oligonucleotides 5'-(6-FAM-NHS)(5'-tyrosine)GATCT(3'-BHQ-1)-3', 5'-phosphotyrosine-GATCTAA AAGACT-3'-(6-FAM)-3' and 5'-phosphotyrosine-GATCTA(Cy5)AAGA CTT-phosphate-3' were purchased from Midland Certified Reagents.

2.3.1. Protein purification, crystallization and structure determination

The humanized zebrafish TDP2 catalytic domain (spanning amino acid residues 120 to 369; 14M_zTdp2^{cat}) was expressed from a codon-optimized gene as a SUMO (Smt3)-fusion protein in the *Escherichia coli* strain BL21(DE3) and purified essentially as described (Shi et al., 2012) using nickel-affinity and size-exclusion chromatography steps. The first residue Asp120 was mutated to Ser to facilitate cleavage by the SUMO-protease Ulp1. The purified protein in 20 mM Tris-HCl (pH 7.4), 150 mM NaCl, 10 mM dithiothreitol was concentrated by ultrafiltration to ~15 mg/mL, flash frozen in liquid nitrogen, and stored in -80°C . Human TDP2 catalytic domain (residues 110–362) was expressed and purified similarly, except that SUMO fused to the N-terminus was kept uncleaved to mitigate the lower solubility of the human enzyme.

14M_zTdp2^{cat} was crystallized by the hanging drop vapor diffusion method using a reservoir solution consisting of 22% polyethylene glycol 3350, 75 mM sodium malonate (pH 7.0), and 0.2 M NaCl. The crystals typically grew as clusters of small and thin plates resembling a pinecone, and they had to be broken into small pieces before being flash

frozen in liquid nitrogen for data collection. The crystals were screened, and x-ray diffraction data collected at the Advanced Photon Source NE-CAT 24 ID-E beamline at the wavelength of 0.979 Å. The diffraction datasets were processed using HKL2000 (Otwinowski and Minor, 1997) and XDS (Kabsch, 2010). Structure was solved by molecular replacement using zebrafish TDP2 structure (PDB ID: 4F1H) as the search model using PHASER program (McCoy et al., 2007). Three copies of TDP2 monomers were located in the asymmetric unit. Initial refinement of the molecular replacement solutions using REFMAC (Murshudov et al., 1997) yield R_{work} and R_{free} of 37% and 41% respectively. Subsequent refinement and model building were done using PHENIX (Adams et al., 2010) and COOT (Emsley et al., 2010). Final R_{work} and R_{free} are 18.3% and 20.9%, respectively. The summary of data collection and model refinement statistics is shown in Table S1 (Supplementary material). Molecular graphic images were produced using PYMOL (www.pymol.org). The atomic coordinates and structure factor amplitudes have been deposited in the Protein Data Bank with accession code 6CA4.

2.3.2. 14M_zTDP2^{cat} fluorescence-based biochemical assay

2.3.2.1. Optimization of assay conditions. All experiments were performed in 384-well costar black plates. The reaction buffer used was composed by 50 mM Tris-HCl pH 7.4, 10 mM MgCl₂, 80 mM KCl, 0.05% (v/v) Tween-20, and 1 mM dithiothreitol (DTT). To optimize enzyme and substrate concentrations, experiments varying the concentration of the enzyme (0–800 pM) as well as experiments varying substrate concentrations (0–50 nM) with fixed concentrations of substrate (1 μ M) and enzyme (6.25 pM) respectively were performed. All experiments were performed with a final reaction volume of 20 μ L: To 10 μ L of enzyme solution, 10 μ L of substrate was added to initiate reaction. The fluorescence of the product was measured using a SpectraMax M5e (Molecular Devices) (λ_{ex} 285 nm; λ_{em} 325 nm; λ_{cutoff} 315 nm) in kinetic-mode at 25 $^{\circ}\text{C}$ for 60–120 min. Assay DMSO tolerance was tested using 10 concentrations of DMSO (0–10%), and IC₅₀ determination of the control (2) was performed by using 12 serial (2-fold) dilution concentrations (0.92–2000 μ M). Three consecutive days experiments were also performed to determine the basic “screenability” of the optimized conditions in the HTS format employed.

2.3.2.2. Screening of the compound library. Compounds were screened at single concentration of 50 μ M (final DMSO concentration of 2.5%) in two different plates. In each plate, maximum (wells containing enzyme, substrate and vehicle DMSO, 32 wells) and minimum controls (without enzyme, 24 wells) were included. To a black 384-well plate, 10 μ L of compound solution (100 μ M) was added, followed by addition of 5 μ L of enzyme (25 pM, final concentration of 6.25 pM). After a pre-incubation period of 10 min, 5 μ L of substrate 5'-(6-FAM-NHS)(5'-tyrosine)GATCT(3'-BHQ-1)-3' (4 μ M, final concentration of 1 μ M) was added, and the reaction was allowed to proceed at 25 $^{\circ}\text{C}$ for 60 min before being stopped by the addition of 5 μ L ethylenediaminetetraacetic acid (EDTA) 0.5 mM, pH = 8. The fluorescence was measured using a SpectraMax M5e (Molecular Devices) (λ_{ex} 285 nm; λ_{em} 325 nm; λ_{cutoff} 315 nm) at 25 $^{\circ}\text{C}$. Compounds were selected as hits in the HTS if they displayed at least 24% enzyme inhibition. In this analysis, two compounds exhibited a percent inhibition lower than -50% (TDP2 activity higher than 150%) and were excluded. In addition, due to solubility issues in DMSO, ten compounds were tested at concentrations lower than 50 μ M.

For follow-up experiments, including IC₅₀ determinations, the same protocol was adopted, with the exception that the plates were analyzed in kinetic-mode, and the fluorescence monitored constantly for 60 min immediately after the reaction was started. When solubility allowed, hits were further analyzed at four concentrations in triplicate (25, 50, 100, and 200 μ M), to test dose-dependent response and their potential interference with the assay. When 50% inhibition was reached up to

200 μM , IC_{50} s were determined when possible.

2.3.2.3. Data analysis. Throughout the assay optimization and validation steps the conditions tested were assessed by statistical parameters: Z' factor, signal-to-background (S:B) and coefficients of variation (%CV) (Inglese et al., 2007; Zhang et al., 1999). These parameters were also calculated during the HTS screen phase to ensure the quality of the data obtained.

$$Z' = 1 - (3 \times \sigma_{\max} + 3 \times \sigma_{\min}) / (\mu_{\max} - \mu_{\min})$$

$$\text{S:B} = \mu_{\max} / \mu_{\min}$$

$$\%CV = \sigma / \mu \times 100$$

In the equations above, μ_{\max} and μ_{\min} represent the mean values of fluorescence for maximum and minimum controls, respectively, and σ_{\max} and σ_{\min} represent their respective standard deviations.

Kinetic parameters (K_m and V_{\max}) were calculated using a non-linear Michaelis-Menten fitting of initial velocities as a function of substrate concentration (GraphPad Prism software). The inhibitory activity of the test compounds was calculated by normalizing the results plate-wise against the controls according to the following equation:

$$\text{Inhibition\%} = [1 - (F_c - \mu_{\min}) / (\mu_{\max} - \mu_{\min})] \times 100$$

In the equation above, F_c is the fluorescence value from an individual test compound well, or in the case of dose-response experiments, the mean value of three technical replicates performed in the same plate. Data from the IC_{50} determination experiments using 10 to 12 concentrations of inhibitor and vehicle-alone were fitted by GraphPad Prism software.

2.3.3. SUMO hTDP2^{cat} fluorescence-based biochemical assay

The reaction buffer used was composed by 50 mM Tris-HCl pH 7.4, 10 mM MgCl_2 , 80 mM KCl, 0.05% (v/v) Tween-20, and 1 mM DTT. To a black 384-well plate, 10 μL of compound solution (in reaction buffer, concentration 2-fold higher than the tested concentration) was added, followed by addition of 5 μL of SUMO hTDP2^{cat} enzyme (12.5 pM, final concentration of 3.13 pM). After a pre-incubation period of 10 min, 5 μL of substrate 5'-(6-FAM-NHS)(5'-tyrosine)GATCT(3'-BHQ-1)-3' (1 μM , final concentration of 0.25 μM) was added, and the reaction was allowed to proceed at 25 °C for 60 min. The fluorescence was measured, and the data was processed as described previously for 14M_zTDP2.

2.3.4. TDP2 gel-based assays.

2.3.4.1. Confirmatory assay. The reaction buffer used was composed by 50 mM Tris-HCl pH 7.4, 10 mM MgCl_2 , 80 mM KCl, and 1 mM DTT. To 6.5 μL of reaction buffer, 1 μL of enzyme solution (15 μM), and 0.5 μL of

inhibitor solution (in DMSO, concentration 20-fold higher than the tested concentration) or DMSO was added and allowed to mix for 10 min. Then, 2 μL of 5'-YGATCTAAAAGACT-3'-(6-FAM)-3' substrate (10 μM) was added, and the reaction was allowed to proceed at 25 °C for 30 min before being stopped by the addition of 10 μL of formamide/bromophenol blue loading buffer. Samples were boiled for 5 min, loaded into 15% polyacrylamide TBE + urea gel, and ran at 200 V for 45 min. Gels were then analyzed by BioRad Gel Doc EZ imager (blue tray 1708273).

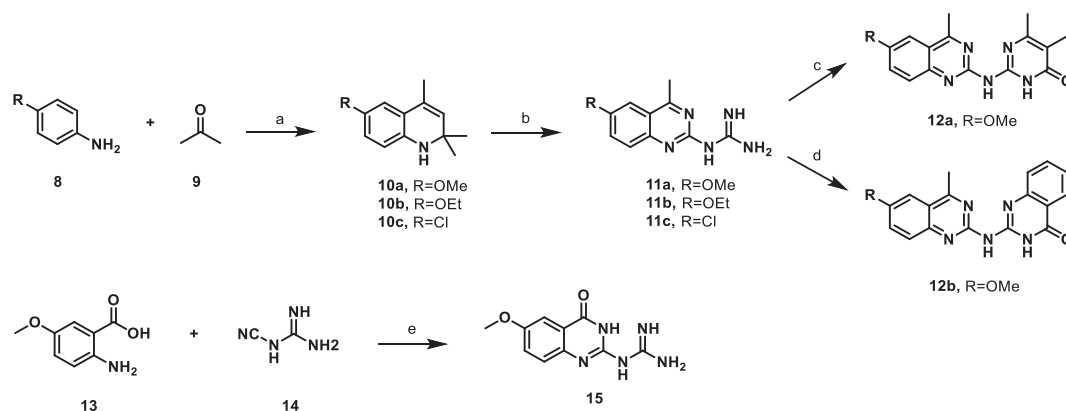
2.3.4.2. WT_zTDP2 and mutants performance evaluation. TDP2 reactions were carried out similarly to describe previously (Gao et al., 2012) with the following modifications. A 14-mer single-stranded oligonucleotide DNA substrate 5'-phosphotyrosine-GATCTA(Cy5)AAGACTT-3'-phosphate containing a 5'-phosphotyrosine (Cy5-Y14) and Cyanine5 (Cy5) dye incorporated in place of the nucleotide at position 7. The Cy5-Y14 was incubated at 40 nM with TDP2 in the absence or presence of an inhibitor for 15 min at room temperature in the reaction buffer containing 50 mM Tris-HCl, pH 7.5, 80 mM KCl, 5 mM MgCl_2 , 0.1 mM EDTA, 1 mM DTT, 40 $\mu\text{g}/\text{mL}$ BSA, and 0.01% Tween 20. Reactions were terminated by the addition of 1 volume of gel loading buffer (5 mM EDTA solution in formamide). Polyacrylamide gels were cast in low fluorescence glass molds. Samples were subjected to a 16% denaturing PAGE. Gels were scanned directly in the mold on a Typhoon™ FLA 9500 (GE Healthcare) scanner using 635 nm excitation light. Densitometry analyses were performed using the ImageQuant software (GE Healthcare).

3. Results and discussion

3.1. Chemistry

Substituted 1,2-dihydro-2,2,4-trimethylquinoline derivatives (**10**, Scheme 1) (Li et al., 2015) were synthesized via modified Skraup reaction by treating substituted anilines with acetone in the presence of catalytic InCl_3 . Acid catalyzed reaction of compound **10** with cyanoguanidine produced the desired 4-methylquinazolyl-2-guanidines analogs (**11**) (Rosowsky and Modest, 1972; Webb et al., 2003) which was further derivatized by treating with diketoester or anthranilic acid in DMF at 170 °C to furnish compounds **12a** (LaPorte et al., 2014) and **12b** (Shikhaliev et al., 2003) respectively. Compound **15** was obtained by the condensation of anthranilic acid derivative (**13**) with cyanoguanidine in refluxing 10% sulfuric acid in a moderate yield.

Reaction of furoic hydrazide (**16**, Scheme 2) with carbon disulfide in methanolic potassium hydroxide at room temperature afforded the dithiocarbazinate derivative (**17**) which subsequently underwent ring



Scheme 1. Synthesis of *N*-quinazolyl-2yl guanidines. (a) InCl_3 (5 mol%) 50 °C, 24 h, 40–65%; (b) cyanoguanidine, HCl conc, H_2O , reflux, 4 h, 55–62%; (c) ethyl 2-methylacetoacetate, DMSO, 170 °C, 30%; (d) Anthranilic acid, DMSO, 170 °C, 64%; (e) H_2SO_4 conc, 100 °C, 55%.

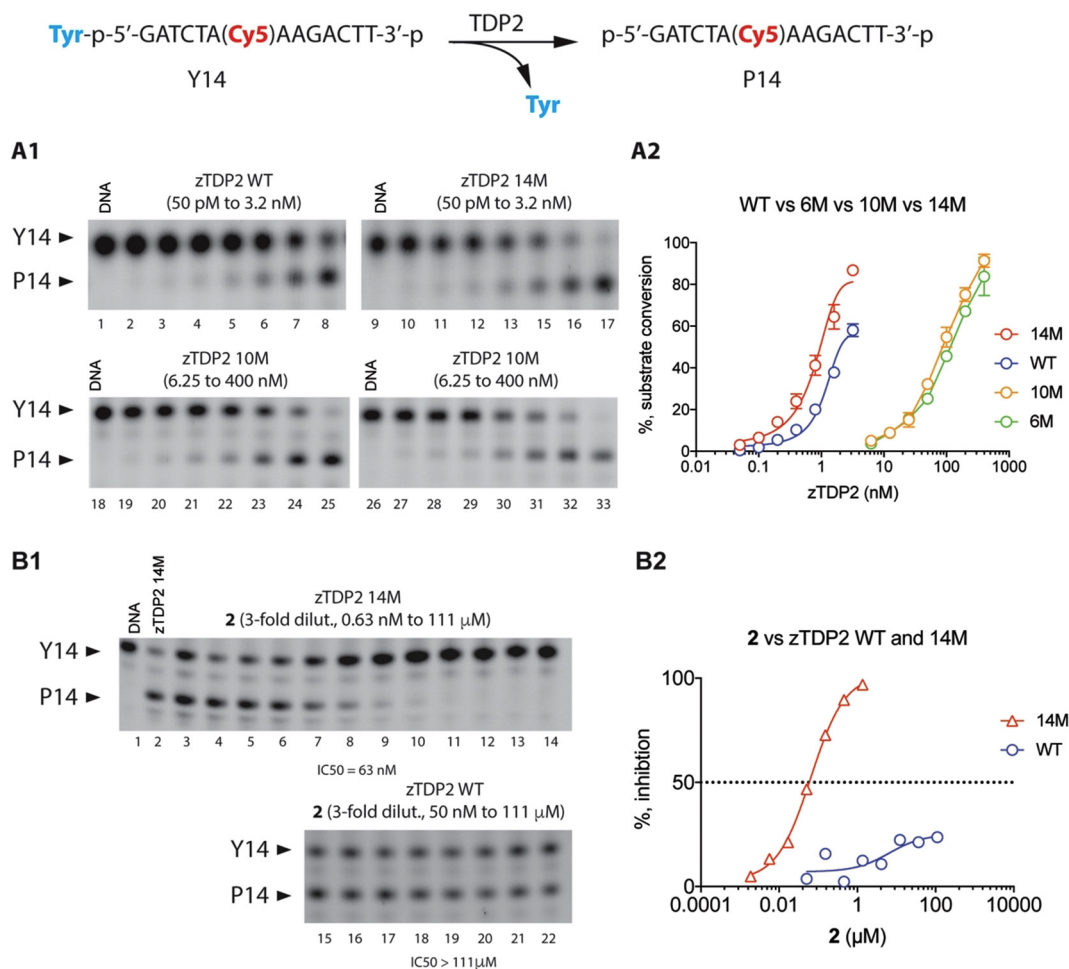
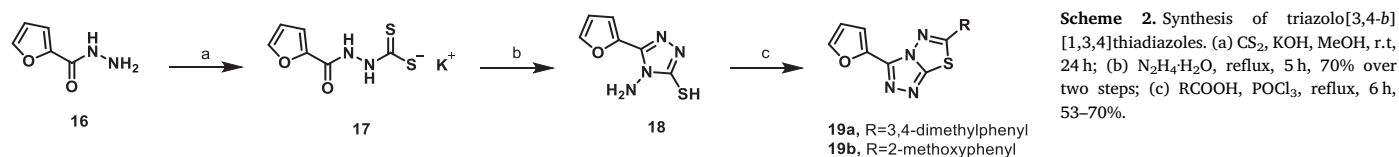


Fig. 2. The humanized 14M_zTDP2 is catalytically as active as the WT enzyme. (A) Hydrolysis of 5'-phosphotyrosyl DNA substrate catalyzed by WT_zTDP2, and the 14M, 6M, 10M mutants. (A1) Representative gels: lanes 1, 9, 18, 26: substrate DNA alone; lanes 2–8: seven 2-fold dilutions of WT_zTDP2 from 3.2 nM to 50 pM; lanes 10–17: seven 2-fold dilutions of 14M_zTDP2 mutant from 3.2 nM to 50 pM; lanes 19–25: seven 2-fold dilutions of 6M_zTDP2 mutant from 400 nM to 6.25 nM; lanes 27–33: seven 2-fold dilutions of 10M_zTDP2 mutant from 400 nM to 6.25 pM. (A2) 5'-Phosphotyrosyl DNA substrate conversion quantification and regression curves, plotted data and SD are based on three independent repeats. (B) Inhibition of zTDP2 (WT and 14M mutant) catalyzed hydrolysis of 5'-phosphotyrosyl DNA substrate by deazaflavin 2. (B1) Representative gels: lane 1: substrate DNA alone; lane 2: substrate DNA with 14M_zTDP2; lanes 3–14: substrate DNA, 14M_zTDP2, and twelve 3-fold dilutions of 2 from 111 μM to 0.63 nM; lanes 15–22: substrate DNA, 14M_zTDP2, eight 3-fold dilutions of 2 from 111 μM to 50 nM. (B2) 5'-Phosphotyrosyl DNA hydrolysis inhibition quantification and regression curves.

closure with an excess of hydrazine monohydrate to give the key triazole intermediate (**18**) (Khan et al., 2016). Condensation of the aryl triazole (**18**) with substituted benzoic acids in phosphorus oxychloride under reflux provided access to the 1,2,4-triazolo[3,4-b][1,3,4]thiadiazoles (**19**) in moderate to excellent yields.

3.2. Development of a protein surrogate: 14M_zTDP2^{cat}

Previous attempts to obtain high-quality crystals of hTDP2 were unsuccessful due to limited solubility of the human protein. Conversely, zTDP2 is a much more soluble protein with suitable crystallographic behavior and that has provided structures with high resolution (Rao et al., 2016; Shi et al., 2012). In addition, the catalytic domains of zebrafish and human TDP2 share high sequence identity (58%) warranting high degree of structural similarity (Shi et al., 2012). Yet, they do not respond similarly to the deazaflavin inhibitors (Marchand et al.,

2016). Thus, to obtain crystal structures relevant for the development of inhibitors against human TDP2, we took the approach to selectively humanize the active site and the DNA-binding groove of zTDP2 by amino acid substitutions and to make a surrogate for hTDP2 with adequate biochemical properties. Recently, Hornyak et al. similarly generated a humanized mouse TDP2 to overcome the problem of poor quality and reproducibility of the hTDP2^{cat} crystals (Hornyak et al., 2016). We also took this approach to make mouse TDP2 sensitive to deazaflavin inhibitors (Marchand et al., 2016).

To achieve our goal of generating humanized zebrafish TDP2 proteins, several surface-exposed residues within ~ 20 Å from the active center were changed to the corresponding human sequence. A series of zTDP2 catalytic domain constructs (residues 120–369) were generated. The three reported here included 6, 10 or 14 amino acid substitutions: 6M (L136N, A139S, C239T, K240R, K314L, C322L), 10M (L136N, A139S, C239T, K240R, K314L, Y318A, V319A, S320C, R321K, C322L)

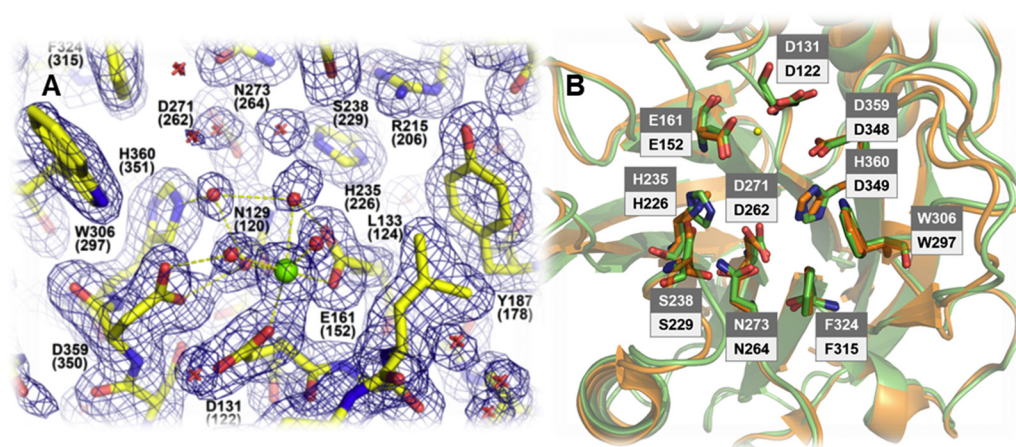


Fig. 3. A) The active site of 14M_zTDP2. 2mFo-DFc electron density map contoured at 1.0 σ is overlaid on the atomic model of the protein shown in sticks. Magnesium ion and coordinating water molecules are represented by small green and red spheres, respectively, with hydrogen bonds or metal-coordinating interactions indicated by yellow dotted lines. Other water molecules are depicted by red crosses. Protein residues are labeled accordingly to the wild type zebrafish TDP2 sequence, with the numbering for the equivalent human TDP2 residues shown in parentheses. B) Superposition of hTDP2 (pdb code: 5J3P) and 14M_zTDP2 (pdb code: 6CA4) in orange and green, respectively, with key active site residues in sticks and labeled as follows: hTDP2 (black text on white background), 14M_zTDP2 (white text on grey back-

ground). (For interpretation of the references to color in this figure legend, the reader is referred to the web version of this article.)

and 14M (L136N, A139S, C239T, K240R, K309Q, K314L, T315G, V316I, P317T, Y318A, V319A, S320C, R321K, and C322L). To survey the performance of the WT_zTDP2 along with its generated 6M, 10M and 14M mutants, we redesigned the assay based on use of ³²P-labeled DNA (Cortes Ledesma et al., 2009; Gao et al., 2012) to employ the fluorophore marker for oligomeric DNA detection. Using this gel-based assay with Cyanine5 (Cy5) dye incorporated into DNA substrate allows for speedier assays by eliminating required substrate 3'-³²P labeling reaction as well as cutting the gel handling steps, i.e. transferring from the mold, drying and exposing. With this assay we verified that only 14M_zTDP2 is catalytically as active as WT_zTDP2 (Fig. 2A), while 6M and 10M mutants turned out to be significantly less active (Fig. 2A). In addition, 14M_zTDP2 is as sensitive as hTDP2 to the known hTDP2 inhibitor 2: hTDP2 IC₅₀ = 40 nM (Marchand et al., 2016; Raouf et al., 2013); 14M_zTDP2 IC₅₀ = 63 nM; zTDP2 IC₅₀ > 100 μ M (Fig. 2B).

We were able to obtain high-quality crystals of 14M_zTDP2, which allowed structure solution at 1.62 \AA resolution (Rfree = 20.9%). The crystal structure of our humanized TDP2 (14M_zTDP2) shows the active site containing a magnesium ion closely resembling those of mouse and zebrafish TDP2 (Fig. 3A). Notably, an extended loop flanking the active site of 14M_zTDP2 appears to be highly flexible, where the residues 312–318 (corresponding to hTDP2 303–309) could not be modeled due to weak electron density. This flexible loop was previously shown to play roles in the binding of DNA (Schellenberg et al., 2012; Shi et al., 2012) and deazaflavin-based inhibitors (Hornyak et al., 2016). A superposition of our structure of 14M_zTDP2 refined at 1.6 \AA resolution with that of hTDP2^{cat} (3.1 \AA resolution) shows high structural similarity as expected, with an r.m.s.d. of 0.47 \AA for all backbone atoms (Fig. 3B). We used this surrogate protein for in silico and biochemical studies.

3.3. Curation of screening compounds

The protein model used for the VHTS was based on the crystal structure of the humanized 14M_zTDP2 (6CA4). 460,000 compounds from Chembridge Library were then run in this model using Glide vHTS and scored based on active site binding. The top 7200 compounds were selected for visual inspection which concerns mostly physicochemical properties and synthetic tractability of ranked compounds. In the end, 1600 small molecules were purchased (Fig. 4).

3.4. Assay optimization

We developed a fluorescence based assay suitable for high throughput screening in 384-well plates. The substrate employed consists of a fluorophore-quencher dual-labeled single stranded 5-mer oligonucleotide (Fig. 5). Specifically, it contains a 5'-tyrosine residue labeled with the donor fluorophore FAM and a 3'-BHQ-1 molecule that

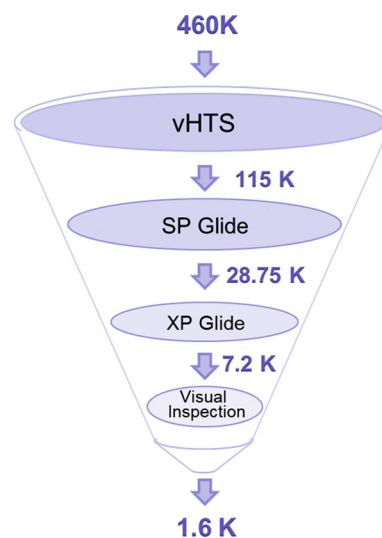


Fig. 4. Schematic representation of the in silico screening campaign. vHTS: virtual high throughput screening; SP: standard precision; XP: extra-precision.

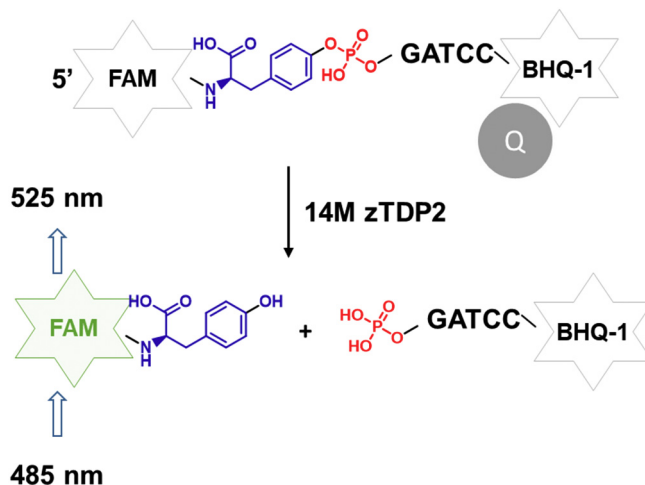


Fig. 5. Schematic representation of the biochemical fluorescence-based assay, employing a fluorophore-quencher dual-labeled substrate. Upon cleavage by humanized 14M_zTDP2^{cat} enzyme, labeled tyrosine is released from the single-stranded oligonucleotide. TDP2 activity is monitored by the increase of fluorescence measured at 525 nm, when FAM is excited at 485 nm. FAM: 6-Carboxyfluorescein; BHQ-1: Black hole quencher-1.

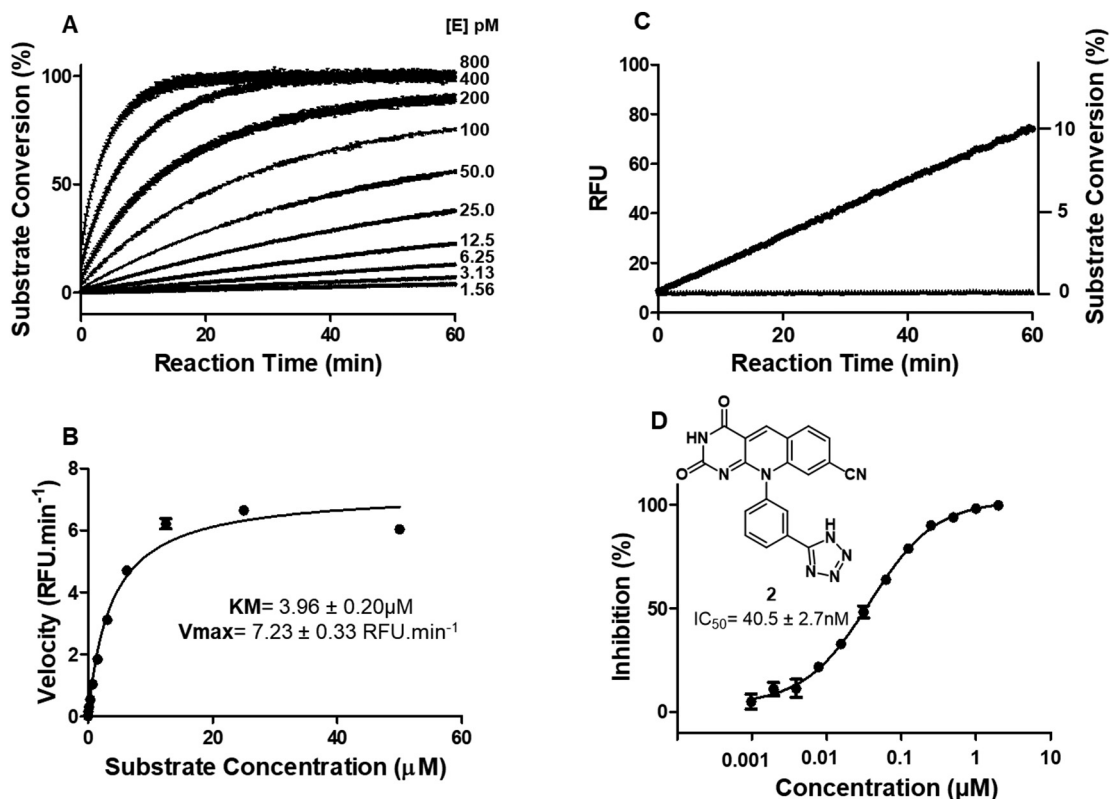


Fig. 6. HTS optimization. (A) Enzyme titration as a function of substrate conversion over reaction time. $[S] = 1 \mu\text{M}$; (B) Michaelis-Menten curve for $14M_z\text{TDP2}^{\text{cat}}$. $[E] = 6.25 \text{ pM}$; (C) Linearity of enzymatic response, when $[E] = 6.25 \text{ pM}$ and $[S] = 1 \mu\text{M}$. $R^2 = 1$; Substrate conversion after 60 min: $10.1 \pm 1.8\%$; S:B = 10 (three independent experiments performed in triplicate); (D) Dose-response curve for the positive control **2**. Km, Vmax, and IC_{50} values are the mean of three independent experiments performed in triplicate, with error bars representing one standard deviation. RFU: Relative fluorescence units.

acts as a dark quencher. The close proximity between FAM and BHQ-1 in the intact substrate allows proper quenching of the energy emitted at 525 nm by FAM when excited at 485 nm. Cleavage of the phosphodiester 5'-phosphotyrosine bond mediated by TDP2 liberates the fluorophore from the quencher effect, and an increase in fluorescence is observed. Therefore, TDP2 activity can be monitored as a function of the fluorescence measured.

We started the optimization by varying protein concentration (0–800 pM) with a fixed amount of substrate (1 μM) over a period of

60 min. This assay allowed us to determine a starting enzyme concentration (6.25 pM) for subsequent kinetic studies that ensured linearity of the fluorescence measured over the duration of the assay (Fig. 6A) To choose the appropriate substrate concentration, we then performed experiments with different substrate amounts (0–50 μM) with the enzyme concentration selected in the preceding step to determine the Michaelis-Menten steady-state kinetic parameters (Km and Vmax) (Fig. 6B). We decided to maintain the sub-Km substrate concentration tested previously (1 μM , $0.25 \times \text{Km}$) that also allowed a

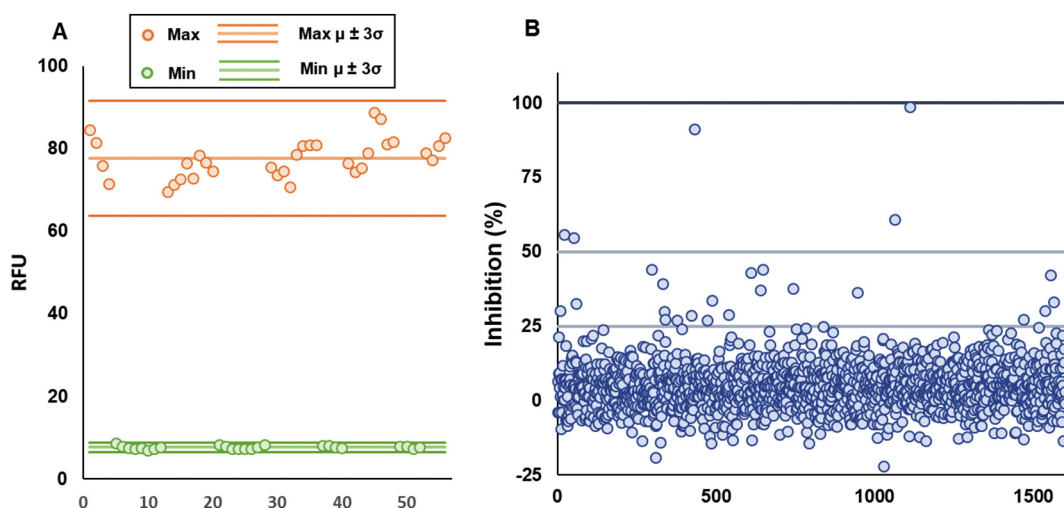


Fig. 7. HTS assays. (A) Example of one plate reading, showing only the maximum (Max, enzyme + substrate) and minimum (Min, substrate only) and their respective average value (μ) and $3 \times$ Standard deviation (3σ) limits. Statistical parameters: $Z' = 0.78$; S:B = 10; intra-plate $\%CV_{\text{Max}} = 6\%$ and $\%CV_{\text{Min}} = 5\%$. Data were plotted first by column, then by row. RFU: Relative fluorescence units (B) Scatter plot showing the percent inhibition for the compound library.

Table 1

Screening hits that showed $\geq 24\%$ inhibition in the screening, and at least 50% inhibition at 200 μM inhibitor concentration.

Compound hits	IC ₅₀ (μM) ^a	Compound hits	IC ₅₀ (μM) ^a
20	18.2 \pm 1.7	27	100 μM : 50 \pm 5% ^b
21	26.5 \pm 0.3	11a	129 \pm 2
19a	33.1 \pm 3.2	28	133 \pm 11
22a	46.3 \pm 9.3	29	150 μM : 51 \pm 2% ^b
23	50 μM : 50 \pm 5% ^b	30	150 μM : 50 \pm 1% ^b
22b	63.2 \pm 0.3	31	200 μM : 56 \pm 5% ^b
24	83.8 \pm 0.9	32	200 μM : 55 \pm 5% ^b
25	85.2 \pm 5.4	33	200 μM : 50 \pm 1% ^b
26	92.0 \pm 14.1		

^{a,b}Values are the means of at least two independent experiments performed in triplicate.

^a Compounds listed according to their IC₅₀ values (chemical structures are presented in Fig. 8).

^b When solubility limitations in the assay conditions prevented accurate IC₅₀ values to be determined, the first concentration tested that reached 50% inhibition is presented, and their chemical structures are reported in Fig. S1 (Supplementary material).

good signal-to-background ratio (10:1), with a low substrate conversion (10.1 \pm 1.8%) (Fig. 6C). In addition, under the established conditions, the assay showed a DMSO tolerance up to 2.5% without significant signal loss (fluorescence variability < 5% from control without DMSO). To verify the accuracy of the inhibition measurements and to confirm the adequate surrogacy of 14M_TDP2^{cat} protein, we determined the IC₅₀ of deazaflavin 2, which has been extensively studied in different biochemical assays (NPPP chromogenic assay IC₅₀ = 40 nM (Raouf et al., 2013); gel-based assay IC₅₀ = 40 \pm 3 nM (Marchand et al., 2016); fluorescence-based assay IC₅₀ = 19 \pm 3.2 nM (Hornyak et al., 2016)). We obtained an IC₅₀ of 40.5 \pm 2.7 nM which is in accordance with literature (Fig. 6D).

Good assay reproducibility and robustness is characterized by high Z'-factors (between 0.5 and 1), low coefficients of variance (lower than 15%) and consistent signal to background (S:B) windows (Inglese et al., 2007; Zhang et al., 1999). Three consecutive days experiments mimicking the HTS conditions revealed a $0.72 \leq Z' \leq 0.81$, intra-plate and inter-plate CV < 10%, and S:B of 9–10.

3.5. HTS and preliminary SAR

A library of 1600 compounds previously curated via virtual screening was screened at a single concentration of 50 μM (Fig. 7). Z'-factors between 0.72 and 0.84 were obtained for all plates, and daily intra-plate and inter-plate CV < 10%. From this library screening, 32 compounds (2% of the library) were selected for further studies (inhibition $\geq 24\%$). First, preliminary studies consisting in experiments involving four compound concentrations (25, 50, 100, and 200 μM , when solubility allowed) were performed, and then for hits with associated dose-dependent inhibition, IC₅₀ values were calculated (Table 1, Fig. 8). To obtain potentially better lead compounds, we eliminated all hits with a steep dose-response curve with slopes > 2 (22b, 24, 25, Fig. 8A), and compounds containing moieties associated with pan assay interference compounds (PAINS). These types of structure are linked to promiscuous bioactivity due to their reactivity nature rather than desired enzyme inhibition (20, 26, 28, Fig. 8B) (Baell and Holloway, 2010; Dahlin and Walters, 2016).

To decide which molecules to move forward to preliminary SAR studies (Fig. 8C), we analyzed their physicochemical properties and determined a few efficiency parameters: ligand efficiency (LE) (Hopkins et al., 2004), lipophilic ligand efficiency (LLE) (Leeson and Springthorpe, 2007; Shultz, 2013), and ligand efficiency dependent lipophilicity (LELP) (Keseru and Makara, 2009) (Table 2). Since TDP2 activities were in the two-three digits micromolar activity range, we

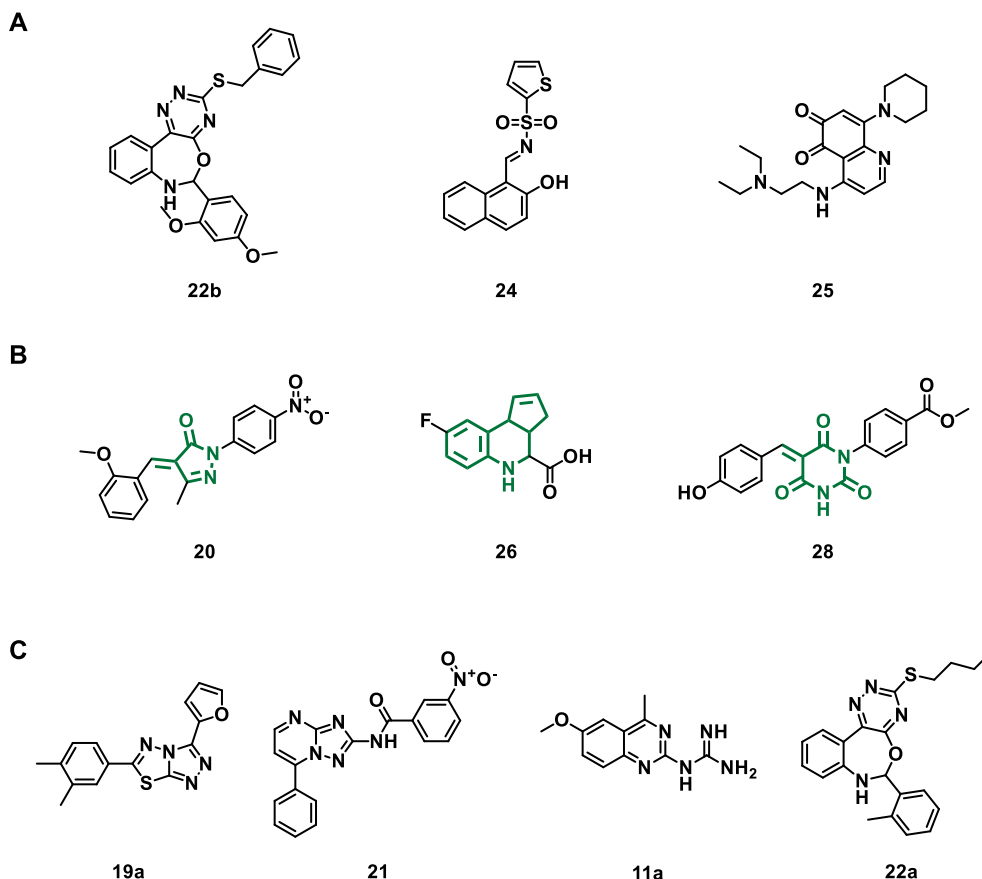


Fig. 8. (A) Compounds with a dose-response slope > 2; (B) Pan assay interference compounds (PAINS); (C) Hit compounds selected for further evaluation.

Table 2

Physicochemical properties and efficiency parameters of selected hits.

Comps	RB ^a	cLogP ^a	tPSA ^a	Hacc ^a	Hdon ^a	MW ^a	LLE ^{a,b}	LE ^{a,c}	LLELP ^{a,d}
11a	2	1.58	96.91	4	3	231.26	2.3	0.32	4.9
19a	4	4.19	56.22	4	0	296.35	0.29	0.30	14
21	3	3.31	115.3	7	1	360.33	1.3	0.24	14
22a	4	4.96	78.39	6	1	378.79	-0.62	0.22	22

^aRB: rotatable bonds; cLogP: logarithm of its partition coefficient between *n*-octanol and water $\log(C_{\text{octanol}}/C_{\text{water}})$; tPSA: topological polar surface area; Hacc: Hydrogen bond acceptor; Hdon: Hydrogen bond donor; MW: molecular weight; LLE: lipophilic ligand efficiency, also referred as LipE; LE: ligand efficiency; LLELP: ligand efficiency dependent lipophilicity.

^bLLE = $\text{pIC}_{50} - \text{cLogP}$.

^cLE = $1.4 \times \text{pIC}_{50} / \text{HAC}$; HAC: heavy atom count (i.e., number of non-hydrogen atoms).

^dLLELP = LE / cLogP .

Non-violations to the rule of three and to the efficiency parameters established are highlighted in grey.

decided to increase the parameters constrains to the Lipinski rule-of-five (Lipinski et al., 2001) to match with what it is typically observed in fragment-based drug design libraries, such as the rule-of-three: MW < 300 Da, normally corresponding to < 20 non-hydrogen atoms; ≤ 3 hydrogen-bond donors and acceptors, ≤ 3 rotatable bonds, $\text{cLogP} \leq 3$, and polar surface area (PSA) $\leq 60 \text{ \AA}^2$ (Congreve et al., 2003; Jhoti et al., 2013). In addition, a good hit in early optimization stages should detain a LLE and a LE of at least 2 and 0.3, respectively, with a LLEP ≤ 10 (Keseru and Makara, 2009; Leach et al., 2006). The HTS hit closer to fulfill these requisites was compound 11a that showed better efficiency parameters despite its lower potency, due presumably to its lower clogP and molecular weight values. The second compound that we selected for further analysis was compound 19a that showed the second-best features in both efficiency parameters and rule-of-three violations.

To confirm the TDP2 inhibition potential of these two hits, we also designed an orthogonal fluorescence gel-based assay that employs

human TDP2^{cat}. As observed in Fig. 9 both hits were able to inhibit the hTDP2 in the same extent as in the primary assay, further corroborating the good surrogacy of 14M_zTDP2 enzyme.

3.5.1. Triazolo[3,4-*b*][1,3,4]thiadiazole derivatives

Recently new biological activities were described for 3,6-diaryl and heteroaryl derivatives of triazolo[3,4-*b*][1,3,4]thiadiazole derivatives (19) such as antitubulin activity (Xu et al., 2017), dCTP pyrophosphatase 1 inhibition (Llona-Minguez et al., 2017), CYP1A1 inhibition (Joshi et al., 2017), and anti-angiogenesis activity by inhibiting TIE-2 (Pan et al., 2015). The observed TDP2 inhibitory activity of hit 19a was confirmed through resynthesizing and retesting (Table 3). This enable us to test an additional 41 triazolo[3,4-*b*][1,3,4]thiadiazole compounds to complement the 24 analogues already present in the 1600 compound library (Table S2, supplementary material). The combined set of 65 compounds was screened at 100 μM . IC₅₀ determination was conducted for derivatives with > 50% inhibition at this concentration (19c–e). We

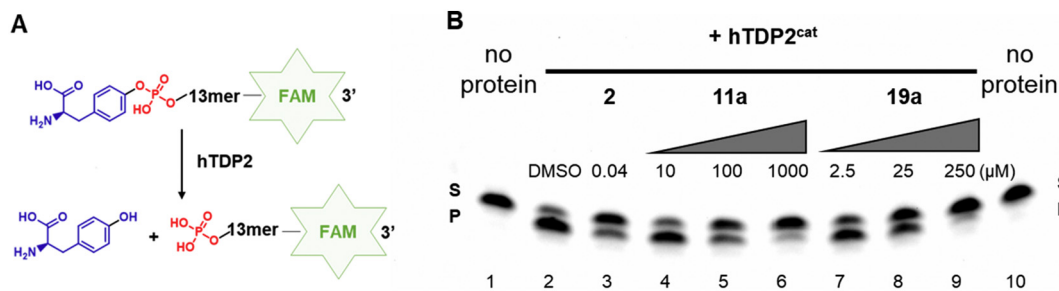


Fig. 9. (A) Schematic representation of the fluorescence gel-based assay. Upon cleavage by SUMO-hTDP2^{cat} enzyme, tyrosine is cleaved from the single-stranded oligonucleotide. Both oligonucleotide substrate and product detain the 3'-fluorophore. FAM: 6-Carboxyfluorescein; (B) Representative gel: lanes 1, 10: substrate DNA only; lane 2: maximum response; lane 3: positive control 2 at IC₅₀ concentration; lanes 4–6: three 10-fold dilutions of hit compound 11a; lanes 7–9: three 10-fold dilutions of hit compound 19a; S: substrate; P: product.

Table 36,7-Dihydrobenzo[*d*][1,2,4]triazino[6,5-*f*][1,3]oxazepane derivatives.

Compound ^a	R ¹	R ²	IC ₅₀ (μM) ^b
19a	3,4-dimethylphenyl	furan-2-yl	20.7 \pm 1.3
19b	2-methoxyphenyl	furan-2-yl	> 100
19c	2-methoxyphenyl	3-methylphenyl	17.6 \pm 0.8
19d	2,4-dichlorophenyl	Pyridin-2-yl	31.5 \pm 1.6
19e	2-methoxyphenyl	2-bromophenyl	74.9 \pm 4.2

Table 4
N-quinazolin-2-yl guanidines derivatives.

Compound ^a	R ¹	R ²	R ³	IC ₅₀ (μM) ^b
11a	6-methoxy	H	-	114 ± 8
11b	6-ethoxy	H	-	150 μM inhibits 50.9 ± 1.1% ^c
11c	6-chloro	H	-	>200
11d	6,7-dimethyl	Benzoyl	-	>200
15	-	-	-	>200
34a	H	H	H	>100
34b	6-methoxy	Methyl	H	>100
34c	6-methyl	Methyl	H	>100
12c	6-methoxy	2-methoxyphenyl	H	25 μM inhibits 58.7 ± 8.1% ^c
12d	8-ethoxy	Methyl	ethyl	19.1 ± 0.3
12a	6-methoxy	Methyl	methyl	22.8 ± 1.9
12b	6-methoxy		Phenyl	27.1 ± 0.3

^aKnown bioactivities for the synthesized compounds against other targets are reported in Table S3 (Supplementary material).

^bValues are the means of three independent experiments performed in triplicate.

^cWhen solubility limitations in the assay conditions prevented accurate IC₅₀ values to be determined, the first concentration tested that reached 50% inhibition is presented.

also synthesized derivative **19b**, which was designed via hybridizing **19a** and **19c/19e**. Yet, **19b** did not exhibit significant TDP2 inhibition at concentrations up to 100 μM. Overall, these preliminary SAR efforts identified a total of 4 derivatives with IC₅₀ lower than 100 μM (Table 3).

^aKnown bioactivities for the synthesized compounds against other targets are reported in Table S3 (Supplementary material).

^bValues are the means of three independent experiments performed in triplicate.

3.5.2. 2-Guanidine-4-methylquinazoline derivatives

2-Guanidine-4-methylquinazoline analogues are associated with a range of biological activities, such as heme enzyme myeloperoxidase inhibition (Soubhye et al., 2017), antibacterial activity by inhibiting translation (Komarova et al., 2017), A type γ-aminobutyric acid receptors (GABA_AR) antagonism (Xiao et al., 2013), acid sensing ion channel ASIC3 activation (Yu et al., 2010), and anti-H₂-histamine activity (Pinelli et al., 1996). Again, hit **11a** was confirmed via re-synthesizing and retesting (Table 4). The initial SAR study focusing on position 6 (**11a–c**) revealed that increasing the length of the ether side chain did not interfere significantly with the activity (**11b** vs. **11a**), whereas changing the substituent to chloro abrogated completely the inhibitory activity up to 200 μM (**11c** vs. **11a**). In addition, no inhibition was observed with the 4-ketone analogue (**15**) synthesized to probe position 4 of the hit compound. Four compounds with derivatization in the guanidine end were already present in the screening library (**11d**, **34a–c**). However, pyrimidine derivatives (**34a–c**) were not able to produce 50% inhibition at 100 μM and higher concentrations were not achievable due to solubility limitations. Although aromatization of the guanidine did not lead to potency improvement, we decided to test pyrimidine derivatives due to their reported biological activities, such as STAT3 pathway inhibition (LaPorte et al., 2014), enhancement of zeste 2 (EZH2) inhibition (Wu et al., 2016), and bacterial DNA

Table 5

Comparison of IC₅₀ values when 14M_zTDP2 and hTDP2 enzymes were employed.

Compound	14M_zTDP2 ^{cat} IC ₅₀ (μM) ^a	SUMO hTDP2 ^{cat} IC ₅₀ (μM) ^a
11a	114 ± 8	113 ± 10
12a	22.8 ± 1.9	17.7 ± 1.7
19a	20.7 ± 1.3	23.6 ± 1.9

^a Values are the means of three independent experiments performed in triplicate.

polymerase III inhibition (Guiles et al., 2009). We purchased and tested two derivatives **12c–d**. Both were at least 5-fold more active than the guanidine hit. This led to the synthesis and testing of two new pyrimidone derivatives (**12a–b**), with the 6-methoxy group of the original hit retained. All pyrimidone derivatives tested were found to be equipotent (IC₅₀ = 17–27 μM).

Lastly, the activity of the hit compounds, as well as the best synthesized guanidine derivative, was confirmed using human TDP2 enzyme in the same biochemical fluorescence-based assay, as similar potencies were observed (Table 5).

4. Conclusions

TDP2 inhibitors can be used to enhance TOP2-targeted drugs (etoposide, doxorubicin, daunorubicin), which are widely used as anticancer therapies. In addition, TDP2 inhibitors could provide novel antiviral strategies for targeting picornaviruses and HBV. To facilitate the discovery of novel TDP2 inhibitor scaffolds, we report here the generation of a humanized zebrafish TDP2 (14M_zTDP2), which provides further structural insights on the TDP2 catalytic site. We show that the 14 M enzyme is sensitive to the reference TDP2 inhibitors of the deazaflavin class, and is readily amenable to biochemical and drug screening studies. Indeed, we developed a new fluorescence-based

biochemical assay suitable for 384-well plate screenings with a simple, homogeneous “mix and read” procedure that allows readings of both continuous and quenched reactions. This assay was used to screen 1600 commercial compounds preselected from 460,000 Cambridge Library compounds through vHTS. Selected hits (**11a** and **19a**) were confirmed using a novel secondary gel-based fluorescence assay with re-synthesized samples. Preliminary SAR studies identified guanidine derivative **12a** (hTDP2 IC₅₀ = 17.7 μM) as an improved inhibitor over the original hit **11a** (hTDP2 IC₅₀ = 113 μM). These results support our new assays (chemical screening and crystallographic analyses) as tools in TDP2 inhibitor discovery.

Acknowledgments

This research was supported by the Academic Health Center Faculty Research Development Grant Program (FRD #14.23), University of Minnesota, and partially by the Center for Drug Design, University of Minnesota, and NIH grant GM118047 to HA. We thank Surajit Banerjee for his assistance during diffraction data collection at the Advanced Photon Source. This work is based upon research conducted at the Northeastern Collaborative Access Team beamlines, which are funded by the National Institute of General Medical Sciences from the National Institutes of Health (P41 GM103403). This research used resources of the Advanced Photon Source, a U.S. Department of Energy (DOE) Office of Science User Facility operated for the DOE Office of Science by Argonne National Laboratory under Contract No. DE-AC02-06CH11357. Studies performed by EK, AG and YP were supported by the Center for Cancer Research, the Intramural Program of the National Cancer Institute (Z001 BC006150).

Appendix A. Supplementary data

Supplementary data to this article can be found online at <https://doi.org/10.1016/j.ejps.2018.03.021>.

References

- Acker, M.G., Auld, D.S., 2014. Considerations for the design and reporting of enzyme assays in high-throughput screening applications. *Perspect. Sci.* 1, 56–73.
- Adams, P.D., Afonine, P.V., Bunkoczi, G., Chen, V.B., Davis, I.W., Echols, N., Headd, J.J., Hung, L.W., Kapral, G.J., Grosse-Kunstleve, R.W., McCoy, A.J., Moriarty, N.W., Oeffner, R., Read, R.J., Richardson, D.C., Richardson, J.S., Terwilliger, T.C., Zwart, P.H., 2010. PHENIX: a comprehensive python-based system for macromolecular structure solution. *Acta Cryst. D* 66, 213–221.
- Adhikari, S., Karmahapatra, S.K., Elias, H., Dhopeshwarkar, P., Williams, R.S., Byers, S., Uren, A., Roy, R., 2011. Development of a novel assay for human tyrosyl DNA phosphodiesterase 2. *Anal. Biochem.* 416, 112–116.
- Baell, J.B., Holloway, G.A., 2010. New substructure filters for removal of pan assay interference compounds (PAINS) from screening libraries and for their exclusion in bioassays. *J. Med. Chem.* 53, 2719–2740.
- Beck, D.E., Lv, W., Abdelmalak, M., Plescia, C.B., Agama, K., Marchand, C., Pommier, Y., Cushman, M., 2016. Synthesis and biological evaluation of new fluorinated and chlorinated indenoisoquinoline topoisomerase I poisons. *Bioorg. Med. Chem.* 24, 1469–1479.
- Brown, J.P., 1965. Reactions of 2,2-dialkyl-1,2-dihydroquinolines. I. Preparation of 2-guanidinoquinazolines. *Monsanto Tech. Revue* 10, 16–18.
- Cain, R., Narramore, S., McPhillie, M., Simmons, K., Fishwick, C.W.G., 2014. Applications of structure-based design to antibacterial drug discovery. *Bioorg. Chem.* 55, 69–76.
- Congreve, M., Carr, R., Murray, C., Jhoti, H., 2003. A ‘rule of three’ for fragment-based lead discovery? *Drug Discov. Today* 8, 876–877.
- Cortes Ledesma, F., El Khamsiy, S.F., Zuma, M.C., Osborn, K., Caldecott, K.W., 2009. A human 5'-tyrosyl DNA phosphodiesterase that repairs topoisomerase-mediated DNA damage. *Nature* 461, 674–678.
- Curtin, N.J., 2012. DNA repair dysregulation from cancer driver to therapeutic target. *Nat. Rev. Cancer* 12, 801–817.
- Dahlin, J.L., Walters, M.A., 2016. How to triage PAINS-full research. *Assay Drug Dev. Technol.* 14, 168–174.
- Do, P.M., Varanasi, L., Fan, S., Li, C., Kubacka, I., Newman, V., Chauhan, P.K., Daniels, S.R., Bocchetta, M., Garrett, M.R., Li, R., Martinez, L.A., 2012. Mutant p53 cooperates with ETS2 to promote etoposide resistance. *Genes Dev.* 26, 830–845.
- Emsley, P., Lohkamp, B., Scott, W.G., Cowtan, K., 2010. Features and development of Coot. *Acta Cryst. D* 66, 486–501.
- Fortune, J.M., Osheroff, N., 2000. Topoisomerase II as a target for anticancer drugs: when enzymes stop being nice. *Prog. Nucleic Acid Res. Mol. Biol.* 64, 221–253.
- Friesner, R.A., Banks, J.L., Murphy, R.B., Halgren, T.A., Klicic, J.J., Mainz, D.T., Repasky, M.P., Knoll, E.H., Shelley, M., Perry, J.K., Shaw, D.E., Francis, P., Shenkin, P.S., 2004. Glide: a new approach for rapid, accurate docking and scoring. 1. Method and assessment of docking accuracy. *J. Med. Chem.* 47, 1739–1749.
- Friesner, R.A., Murphy, R.B., Repasky, M.P., Frye, L.L., Greenwood, J.R., Halgren, T.A., Sanschagrin, P.C., Mainz, D.T., 2006. Extra precision glide: docking and scoring incorporating a model of hydrophobic enclosure for protein-ligand complexes. *J. Med. Chem.* 49, 6177–6196.
- Gao, R., Huang, S.Y., Marchand, C., Pommier, Y., 2012. Biochemical characterization of human tyrosyl-DNA phosphodiesterase 2 (TDP2/TTRAP): a Mg(2+)/Mn(2+)-dependent phosphodiesterase specific for the repair of topoisomerase cleavage complexes. *J. Biol. Chem.* 287, 30842–30852.
- Gomez-Herreros, F., Romero-Granados, R., Zeng, Z., Alvarez-Quilon, A., Quintero, C., Ju, L., Umans, L., Vermeire, L., Huylebroeck, D., Caldecott, K.W., Cortes-Ledesma, F., 2013. TDP2-dependent non-homologous end-joining protects against topoisomerase II-induced DNA breaks and genome instability in cells and in vivo. *PLoS Genet.* 9, e1003226.
- Guiles, J., Sun, X., Critchley, I.A., Ochsner, U., Tregay, M., Stone, K., Bertino, J., Green, L., Sabin, R., Dean, F., Dallmann, H.G., McHenry, C.S., Janjic, N., 2009. Quinazolin-2-ylamino-quinazolin-4-ols as novel non-nucleoside inhibitors of bacterial DNA polymerase III. *Bioorg. Med. Chem. Lett.* 19, 800–802.
- Ho, N.N., Shimizu, T., Zhou, Z.W., Wang, Z.Q., Deshpande, R.A., Paull, T.T., Akter, S., Tsuda, M., Furuta, R., Tsutsui, K., Takeda, S., Sasanuma, H., 2016. Mre11 is essential for the removal of lethal topoisomerase 2 covalent cleavage complexes. *Mol. Cell* 64, 580–592.
- Hopkins, A.L., Groom, C.R., Alex, A., 2004. Ligand efficiency: a useful metric for lead selection. *Drug Discov. Today* 9, 430–431.
- Hornyak, P., Askwith, T., Walker, S., Komulainen, E., Paradowski, M., Pennicott, L.E., Bartlett, E.J., Brissett, N.C., Raoof, A., Watson, M., Jordan, A.M., Ogilvie, D.J., Ward, S.E., Atack, J.R., Pearl, L.H., Caldecott, K.W., Oliver, A.W., 2016. Mode of action of DNA-competitive small molecule inhibitors of tyrosyl DNA phosphodiesterase 2. *Biochem. J.* 473, 1869–1879.
- Inglese, J., Johnson, R.L., Simeonov, A., Xia, M., Zheng, W., Austin, C.P., Auld, D.S., 2007. High-throughput screening assays for the identification of chemical probes. *Nat. Chem. Biol.* 3, 466–479.
- Jhoti, H., Williams, G., Rees, D.C., Murray, C.W., 2013. The ‘rule of three’ for fragment-based drug discovery: where are we now? *Nat. Rev. Drug Discov.* 12 (6), 644–644.
- Joshi, P., McCann, G.J.P., Sonawane, V.R., Vishwakarma, R.A., Chaudhuri, B., Bharate, S.B., 2017. Identification of potent and selective CYP1A1 inhibitors via combined ligand and structure-based virtual screening and their in vitro validation in sacchromyces and live human cells. *J. Chem. Inf. Model.* 57, 1309–1320.
- Kabsch, W., 2010. XDS. *Acta Cryst. D* 66, 125–132.
- Kankanala, J., Marchand, C., Abdelmalak, M., Aihara, H., Pommier, Y., Wang, Z., 2016. Isoquinoline-1,3-diones as selective inhibitors of tyrosyl DNA phosphodiesterase II (TDP2). *J. Med. Chem.* 59, 2734–2746.
- Keseru, G.M., Makara, G.M., 2009. The influence of lead discovery strategies on the properties of drug candidates. *Nat. Rev. Drug Discov.* 8, 203–212.
- Khan, I., Panini, P., Khan, S.U.-D., Rana, U.A., Andleeb, H., Chopra, D., Hameed, S., Simpson, J., 2016. Exploiting the role of molecular electrostatic potential, deformation density, topology, and energetics in the characterization of S...N and Cl...N supramolecular motifs in crystalline triazolothiadiazoles. *Crys. Growth Des.* 16, 1371–1386.
- Komarova, E.S., Osterman, I.A., Pletnev, P.I., Ivanenkov, Y.A., Majouga, A.G., Bogdanov, A.A., Sergiev, P.V., 2017. 2-Guanidino-quinazolines as a novel class of translation inhibitors. *Biochimie* 133, 45–55.
- Koniger, C., Wingert, I., Marsmann, M., Rosler, C., Beck, J., Nassal, M., 2014. Involvement of the host DNA-repair enzyme TDP2 in formation of the covalently closed circular DNA persistence reservoir of hepatitis B viruses. *Proc. Natl. Acad. Sci. U. S. A.* 111, E4244–E4253.
- Kont, Y.S., Dutta, A., Mallisetty, A., Mathew, J., Minas, T., Kraus, C., Dhopeshwarkar, P., Kallakury, B., Mitra, S., Uren, A., Adhikari, S., 2016. Depletion of tyrosyl DNA phosphodiesterase 2 activity enhances etoposide-mediated double-strand break formation and cell killing. *DNA Repair* 43, 38–47.
- Koparr, M., Cansiz, A., Demirdag, A., 2004. Synthesis of some new 4,5-substituted-4H-1,2,4-triazole-3-thiol derivatives. *Molecules* 9, 204.
- Kossmann, B.R., Abdelmalak, M., Lopez, S., Tender, G., Yan, C., Pommier, Y., Marchand, C., Ivanov, I., 2016. Discovery of selective inhibitors of tyrosyl-DNA phosphodiesterase 2 by targeting the enzyme DNA-binding cleft. *Bioorg. Med. Chem. Lett.* 26, 3232–3236.
- Laev, S.S., Salakhutdinov, N.F., Lavrik, O.I., 2016. Tyrosyl-DNA phosphodiesterase inhibitors: progress and potential. *Bioorg. Med. Chem.* 24, 5017–5027.
- LaPorte, M.G., da Paz Lima, D.J., Zhang, F., Sen, M., Grandis, J.R., Camarco, D., Hua, Y., Johnston, P.A., Lazo, J.S., Resnick, L.O., Wipf, P., Huryn, D.M., 2014. 2-Guanidinoquinazolines as new inhibitors of the STAT3 pathway. *Bioorg. Med. Chem. Lett.* 24, 5081–5085.
- Leach, A.R., Hann, M.M., Burrows, J.N., Griffen, E.J., 2006. Fragment screening: an introduction. *Mol. Biosyst.* 2, 429–446.
- Leeson, P.D., Springthorpe, B., 2007. The influence of drug-like concepts on decision-making in medicinal chemistry. *Nat. Rev. Drug Discov.* 6, 881–890.
- Li, Y., Wu, C., Huang, J., Su, W., 2006. Mild and convenient synthesis of 1,2-dihydroquinolines from anilines and acetone catalyzed by ytterbium(III) triflate in ionic liquids. *Synth. Commun.* 36, 3065–3073.
- Li, C., Fan, S., Owonikoko, T.K., Khuri, F.R., Sun, S.Y., Li, R., 2011. Oncogenic role of EAPII in lung cancer development and its activation of the MAPK-ERK pathway. *Oncogene* 30, 3802–3812.
- Li, G., Liu, H., Lv, G., Wang, Y., Fu, Q., Tang, Z., 2015. Enantioselective organocatalytic

- transfer hydrogenation of 1,2-dihydroquinoline through formation of aza-o-xylylene. *Org. Lett.* 17, 4125–4127.
- Lipinski, C.A., Lombardo, F., Dominy, B.W., Feeney, P.J., 2001. Experimental and computational approaches to estimate solubility and permeability in drug discovery and development settings. *Adv. Drug Deliv. Rev.* 46, 3–26.
- Llona-Minguez, S., Höglund, A., Witta, E., Almlöf, I., Mateus, A., Calderón-Montaña, J.M., Cazares-Körner, C., Homan, E., Loseva, O., Baranczewski, P., Jemth, A.-S., Häggblad, M., Martens, U., Lundgren, B., Artursson, P., Lundbäck, T., Jenmalm Jensen, A., Warpman Berglund, U., Scobie, M., Helleday, T., 2017. Identification of triazolothiadiazoles as potent inhibitors of the dCTP pyrophosphatase 1. *J. Med. Chem.* 60, 2148–2154.
- Maciejewski, S., Nguyen, J.H.C., Gomez-Herreros, F., Cortes-Ledesma, F., Caldecott, K.W., Semler, B.L., 2016. Divergent requirement for a DNA repair enzyme during enterovirus infections. *MBio* 7.
- Maede, Y., Shimizu, H., Fukushima, T., Kogame, T., Nakamura, T., Miki, T., Takeda, S., Pommier, Y., Murai, J., 2014. Differential and common DNA repair pathways for topoisomerase I- and II-targeted drugs in a genetic DT40 repair cell screen panel. *Mol. Cancer Ther.* 13, 214–220.
- Marchand, C., Abdelmalak, M., Kankanala, J., Huang, S.Y., Kiselev, E., Fesen, K., Kurahashi, K., Sasanuma, H., Takeda, S., Aihara, H., Wang, Z., Pommier, Y., 2016. Deazaflavin inhibitors of tyrosyl-DNA phosphodiesterase 2 (TDP2) specific for the human enzyme and active against cellular TDP2. *ACS Chem. Biol.* 11, 1925–1933.
- McCoy, A.J., Grosse-Kunstleve, R.W., Adams, P.D., Winn, M.D., Storoni, L.C., Read, R.J., 2007. Phaser crystallographic software. *J. Appl. Crystallogr.* 40, 658–674.
- Menon, V., Povirk, L.F., 2016. End-processing nucleases and phosphodiesterases: an elite supporting cast for the non-homologous end joining pathway of DNA double-strand break repair. *DNA Repair (Amst)* 43, 57–68.
- Murshudov, G.N., Vagin, A.A., Dodson, E.J., 1997. Refinement of macromolecular structures by the maximum-likelihood method. *Acta Crystallogr. D Biol. Crystallogr.* 53, 240–255.
- Nitiss, J.L., 2009. DNA topoisomerase II and its growing repertoire of biological functions. *Nat. Rev. Cancer* 9, 327–337.
- Otwinowski, Z., Minor, W., 1997. Processing of X-ray diffraction data collected in oscillation mode. *Methods Enzymol.* 276, 307–326.
- Pan, P., Tian, S., Sun, H., Kong, X., Zhou, W., Li, D., Li, Y., Hou, T., 2015. Identification and preliminary SAR analysis of novel type-I inhibitors of TIE-2 via structure-based virtual screening and biological evaluation in *in vitro* models. *J. Chem. Inf. Model.* 55, 2693–2704.
- Pei, H., Yordy, J.S., Leng, Q., Zhao, Q., Watson, D.K., Li, R., 2003. EAPII interacts with ETS1 and modulates its transcriptional function. *Oncogene* 22, 2699–2709.
- Pinelli, A., Trivulzio, S., Pojaga, G., Rossoni, G., 1996. Effects of 2-guanidino-4-methylquinazoline on gastric acid secretion in rats. *Pharmacol. Res.* 34, 225–230.
- Pommier, Y., 2013. Drugging topoisomerases: lessons and challenges. *ACS Chem. Biol.* 8, 82–95.
- Pommier, Y., Huang, S.-Y.N., Gao, R., Das, B.B., Murai, J., Marchand, C., 2014. Tyrosyl-DNA-phosphodiesterases (TDP1 and TDP2). *DNA Repair* 19, 114–129.
- Pommier, Y., Sun, Y., Huang, S.N., Nitiss, J.L., 2016. Roles of eukaryotic topoisomerases in transcription, replication and genomic stability. *Nat. Rev. Mol. Cell Biol.* 17, 703–721.
- Pype, S., Declercq, W., Ibrahim, A., Michiels, C., Van Rietschoten, J.G., Dewulf, N., de Boer, M., Vandenebeele, P., Huylebroeck, D., Remacle, J.E., 2000. TTRAP, a novel protein that associates with CD40, tumor necrosis factor (TNF) receptor-75 and TNF receptor-associated factors (TRAFs), and that inhibits nuclear factor-kappa B activation. *J. Biol. Chem.* 275, 18586–18593.
- Rao, T., Gao, R., Takada, S., Al Abo, M., Chen, X., Walters, K.J., Pommier, Y., Aihara, H., 2016. Novel TDP2-ubiquitin interactions and their importance for the repair of topoisomerase II-mediated DNA damage. *Nucleic Acids Res.* 44, 10201–10215.
- Raouf, A., Depledge, P., Hamilton, N.M., Hamilton, N.S., Hitchin, J.R., Hopkins, G.V., Jordan, A.M., Maguire, L.A., McGonagle, A.E., Mould, D.P., Rushbrooke, M., Small, H.F., Smith, K.M., Thomson, G.J., Turlais, F., Waddell, I.D., Waszkowicz, B., Watson, A.J., Ogilvie, D.J., 2013. Toxoflavins and deazaflavins as the first reported selective small molecule inhibitors of tyrosyl-DNA phosphodiesterase II. *J. Med. Chem.* 56, 6352–6370.
- Ravindranathan, K.P., Mandiyan, V., Ekkati, A.R., Bae, J.H., Schlessinger, J., Jorgensen, W.L., 2010. Discovery of novel fibroblast growth factor receptor 1 kinase inhibitors by structure-based virtual screening. *J. Med. Chem.* 53, 1662–1672.
- Rosowsky, A., Modest, E.J., 1972. Chemical and biological studies on dihydro-s-triazines .16. NMR evidence for formation of 2-guanidino-4-methylquinazolines as anomalous by-products in 3-component synthesis. *J. Heterocycl. Chem.* 9 (637&).
- Schellenberg, M.J., Appel, C.D., Adhikari, S., Robertson, P.D., Ramsden, D.A., Williams, R.S., 2012. Mechanism of repair of 5'-topoisomerase II-DNA adducts by mammalian tyrosyl-DNA phosphodiesterase 2. *Nat. Struct. Mol. Biol.* 19, 1363–1371.
- Schrödinger, 2014a. Schrödinger Release 2014-3: LigPrep, Version 3.1. Schrödinger, LLC, New York, NY.
- Schrödinger, 2014b. Schrödinger Release 2014-3: Schrödinger Suite 2014-3. (a) Protein Preparation Wizard. (b) Epik version 2.9; Schrödinger, LLC: New York, NY, 2014. (c) Impact version 6.4; Schrödinger, LLC: New York, NY, 2014. (d) Prime version 3.7; Schrödinger, LLC: New York, NY.
- Shi, K., Kurahashi, K., Gao, R., Tsutakawa, S.E., Tainer, J.A., Pommier, Y., Aihara, H., 2012. Structural basis for recognition of 5'-phosphotyrosine adducts by Tdp2. *Nat. Struct. Mol. Biol.* 19, 1372–1377.
- Shikhaliyev, K.S., Krylskii, D.V., Shestakov, A.S., Falaleev, A.V., 2003. Condensation of isatoic anhydride with hetarylguanidines. *Russ. J. Gen. Chem.* 73, 1147–1150.
- Shultz, M.D., 2013. Setting expectations in molecular optimizations: strengths and limitations of commonly used composite parameters. *Bioorg. Med. Chem. Lett.* 23, 5980–5991.
- Simmons, K.J., Chopra, I., Fishwick, C.W., 2010. Structure-based discovery of anti-bacterial drugs. *Nat. Rev. Microbiol.* 8, 501–510.
- Soubhye, J., Chikh Alard, I., Aldib, I., Prévost, M., Gelbcke, M., De Carvalho, A., Furtmüller, P.G., Obinger, C., Flemmig, J., Tadrent, S., Meyer, F., Rousseau, A., Nève, J., Mathieu, V., Zouaoui Boudjeltia, K., Dufresne, F., Van Antwerpen, P., 2017. Discovery of novel potent reversible and irreversible myeloperoxidase inhibitors using virtual screening procedure. *J. Med. Chem.* 60, 6563–6586.
- Theiling, L.F., McKee, R.L., 1952. 2-Guanidinoquinazolines. *J. Am. Chem. Soc.* 74, 1834–1836.
- Thomson, G., Watson, A., Caldecott, K., Denny, O., Depledge, P., Hamilton, N., Hopkins, G., Jordan, A., Morrow, C., Raouf, A., Waddell, I., Ogilvie, D., 2013. Generation of assays and antibodies to facilitate the study of human 5'-tyrosyl DNA phosphodiesterase. *Anal. Biochem.* 436, 145–150.
- Umamaheswari, A., Pradhan, D., Hemanthkumar, M., 2010. Identification of potential *Leptospira* phosphoheptose isomerase inhibitors through virtual high-throughput screening. *Genomics Proteomics Bioinforma.* 8, 246–255.
- Virgen-Slane, R., Rozovics, J.M., Fitzgerald, K.D., Ngo, T., Chou, W., van Noort, G.J.V., Filippov, D.V., Gershon, P.D., Semler, B.L., 2012. An RNA virus hijacks an incognito function of a DNA repair enzyme. *Proc. Natl. Acad. Sci. U. S. A.* 109, 14634–14639.
- Wang, P., Elsayed, M.S.A., Plescia, C.B., Ravji, A., Redon, C.E., Kiselev, E., Marchand, C., Zeleznik, O., Agama, K., Pommier, Y., Cushman, M., 2017. Synthesis and biological evaluation of the first triple inhibitors of human topoisomerase I, tyrosyl-DNA phosphodiesterase 1 (tdp1), and tyrosyl-DNA phosphodiesterase 2 (tdp2). *J. Med. Chem.* 60, 3275–3288.
- Webb, T.R., Lvovskiy, D., Kim, S.-A., Ji, X.-D., Melman, N., Linden, J., Jacobson, K.A., 2003. Quinazolines as adenosine receptor antagonists: SAR and selectivity for A2B receptors. *Bioorg. Med. Chem.* 11, 77–85.
- Wu, Y., Hu, J., Ding, H., Chen, L., Zhang, Y., Liu, R., Xu, P., Du, D., Lu, W., Liu, J., Liu, Y., Liu, Y.-C., Lu, J., Zhang, J., Yao, Z., Luo, C., 2016. Identification of novel EZH2 inhibitors through pharmacophore-based virtual screening and biological assays. *Bioorg. Med. Chem. Lett.* 26, 3813–3817.
- Xiao, X., Zhu, M.X., Xu, T.-L., 2013. 2-Guanidino-4-methylquinazoline acts as a novel competitive antagonist of A type γ -aminobutyric acid receptors. *Neuropharmacology* 75, 126–137.
- Xu, Q., Sun, M., Bai, Z., Wang, Y., Wu, Y., Tian, H., Zuo, D., Guan, Q., Bao, K., Wu, Y., Zhang, W., 2017. Design, synthesis and bioevaluation of antitubulin agents carrying diaryl-5,5-fused-heterocycle scaffold. *Eur. J. Med. Chem.* 139, 242–249.
- Yu, Y., Chen, Z., Li, W.-G., Cao, H., Feng, E.-G., Yu, F., Liu, H., Jiang, H., Xu, T.-L., 2010. A nonproton ligand sensor in the acid-sensing ion channel. *Neuron* 68, 61–72.
- Zeng, Z., Cortés-Ledesma, F., El Khamisy, S.F., Caldecott, K.W., 2011. TDP2/TTRAP is the major 5'-tyrosyl DNA phosphodiesterase activity in vertebrate cells and is critical for cellular resistance to topoisomerase II-induced DNA damage. *J. Biol. Chem.* 286, 403–409.
- Zhang, J.H., Chung, T.D., Oldenburg, K.R., 1999. A simple statistical parameter for use in evaluation and validation of high throughput screening assays. *J. Biomol. Screen.* 4, 67–73.
- Zhang, L.-X., Zhang, A.-J., Chen, X.-X., Lei, X.-X., Nan, X.-Y., Chen, D.-Y., Zhang, Z.-Y., 2002. Synthesis and biological activity of 3-(2-furanyl)-6-aryl-1,2,4-triazolo[3,4-b]-1,3,4-thiadiazoles. *Molecules* 7, 681.